ELSEVIER

Journal of Nuclear Materials 278 (2000) 20–29

journal of nuclear materials

www.elsevier.nl/locate/jnucmat

Fe–15Ni–13Cr austenitic stainless steels for fission and fusion reactor applications. III. Phase stability during heavy ion irradiation

E.H. Lee *, L.K. Mansur

Metals and Ceramics Division, Oak Ridge National Laboratory, P.O. Box 2008, Oak Ridge, TN 37831-6376, USA

Received 3 May 1999; accepted 13 September 1999

Abstract

The phase stability in Fe–15Ni–13Cr alloys was investigated as a function of minor alloying additions after 4 MeV Ni ion irradiation at 948 K. The results showed that the stability of precipitate phases was dictated mainly by the defects produced by radiation damage and preferential segregation of Si and Ni at defects. In addition, radiation enhanced diffusion and cascade induced dissolution and mixing allowed kinetically sluggish phases to form rapidly under irradiation. These radiation effects caused an enhancement, retardation, or modification of thermal phases, and formation of new phases. The relative stability of precipitate phases varied sensitively with alloy composition. The roles of each alloying element on phase stability and the impact of radiation on the mechanisms of phase evolution were systematically studied and documented. The knowledge obtained from this work provides guidelines for designing alloys that lead to develop desired precipitate microstructures under irradiation.

PACS: 64.75.+g; 81.30.Mh; 61.80.-x

1. Introduction

The understanding of phase stability under irradiation is very important to both fission and fusion reactor materials design, because segregation and precipitation lead directly to changes in swelling and mechanical properties. Moreover, the phase stability under irradiation is considerably different from thermal behavior due to radiation induced processes such as enhanced diffusion [1], cascade dissolution [2–4], cascade mixing [5,6], and segregation of various alloying elements [7–10]. Although quite extensive data were documented for the precipitate phases developed under thermal [11] and irradiation [12,13] environments, the data were gathered from various alloy sources. A systematic study with a common base alloy to unveil the effects of minor alloying elements on phase stability is still lacking.

During irradiation, the ability of alloys to sustain the necessary dimensional and mechanical properties to meet design lifetimes and performance is largely dependent upon the manner in which displaced atoms and transmutation helium are accommodated in the microstructure. It was demonstrated that precipitation behavior during irradiation is of major significance because of the relationship between precipitation and swelling behavior [14,15]. It is also realized that precipitation cannot be avoided in multicomponent alloys of technological interest, and that satisfactory alloy performance can be attained only through proper tailoring of precipitate phases. In this work, therefore, an investigation was carried out to understand the phase evolution under irradiation in the Fe–15Ni–13Cr alloy system by systematically varying minor alloying elements.

2. Experimental

The compositions and thermal properties of 28 alloys investigated in this work were described in Parts I and

* Corresponding author. Tel. : +1-423 574 5058; fax: +1-423 574 0641.

E-mail address: leeEH@ornl.gov (E.H. Lee).

0022-3115/00/$ - see front matter
PII: S0022-3115(99)00236-6

II. Detailed alloy fabrication procedures were described in Part I, and precipitate phases produced under thermal aging were summarized in Part II. To investigate the precipitate phases evolving during irradiation, specimen disks (3 mm diameter by 0.35 mm thick) were prepared by solution annealing at1373 K. The annealed specimens were bombarded with 4 MeV Ni ions to irradiation doses of 1 and 70 dpa at 948K (675°C) using the triple ion facility (TIF) at ORNL. Some of the specimens were bombarded simultaneously with He and Ni ions. The irradiated specimen disks were then thinned to expose the peak damage region, 0.6–0.8 μm below the surface, for TEM examination. A JEM-120CX analytical electron microscope equipped with an energy dispersive spectrometer was used for analysis. After in-foil analyses of damage microstructure, diffraction patterns, precipitate orientations, and particle compositions for the various precipitate phases were obtained using the carbon replica extraction technique. The compositions and diffraction patterns of extracted particles were recorded, analyzed, and compared with the in-foil data. The general procedures have been described in a previous paper [12].

3. Results

Ten major precipitate phases were found in irradiated specimens. Of these, $M_{23}C_6$, η-phase, TiO, MC, NbC, and M_2P were also found in thermally aged samples, but their relative volume fraction and composition were in most cases altered by radiation. Four new phases, G, γ′, Ni-rich-γ, and CrSi, were also identified in irradiated specimens. Table 1 summarizes the precipitate phases found in each alloy. The qualitative abundances of precipitate phases are indicated by inequality signs. Typical compositions of precipitate phases are listed in Table 2. The details are described in the following.

3.1. $M_{23}C_6$

$M_{23}C_6$ phase was present in all carbon-containing alloys after irradiation, but generally there was less compared with specimens aged for 24 h at 948 K, except for four Ti and C containing alloys, B5(Ti,C), B6(Ti,C,Mo), B7(Ti,C,Si), and B8(Ti,C,B). In these alloys, there was more $M_{23}C_6$ and TiO formation. TiC was reduced, with the largest effect being seen in alloy B6. The apparent source of the oxygen for the formation of TiO was the dissociation of prior Cr_2O_3 oxide particles during irradiation. During thermal aging, both TiO and $M_{23}C_6$ were suppressed in these same alloys by the formation of TiC.

Fig. 1 compares precipitate phases extracted from thermally aged and irradiated B6 alloy specimens: MC dominates the thermally aged microstructure, and lath-shaped $M_{23}C_6$ and cuboidal TiO particles dominate the irradiated microstructure. EDS analyses showed that $M_{23}C_6$ compositions were virtually unchanged by radiation compared with those formed thermally. Mo-free or Mo-containing $M_{23}C_6$ precipitates were found depending upon the presence of molybdenum in the alloy. $M_{23}C_6$ phase was detected only in trace amounts after irradiation in alloys containing niobium, consistent with niobium carbide being much more stable than $M_{23}C_6$, even under irradiation conditions. Although $M_{23}C_6$ formation increased in alloys with phosphorous during thermal aging due to the formation of Ti-rich

Table 1
Precipitate phases in specimens irradiated with Ni ions to 70 dpa at 948 K

Alloys (additions)[a]	Precipitate phases	Alloys (additions)	Precipitate phases
B1(ternary)	No new phase	E1 (all additions)	MC > G, η
B2 (Ti)	TiO	E2 (−Mo)[b]	MC > G
B3 (Si)	Ni-rich γ ≫ CrSi	E3 (−Mn)	MC > G, η
B4 (B)	No new phase	E4 (−Ti)	No new phase
B5 (Ti, C)	TiO ≫ MC ≫ $M_{23}C_6$	E5 (−C)	TiO, γ′
B6 (Ti, C, Mo)	TiO ≫ $M_{23}C_6$ ≫ MC	E6 (0.3Si)	MC
B7 (Ti, C, Si)	TiO ≫ MC ≫ $M_{23}C_6$	E7 (−Si)	C
B8 (Ti, C, B)	TiO ≫ MC ≫ $M_{23}C_6$	E8 (0.8Si, P)	M_2P ≫ G, MC
B9 (P)	M_2P	E9 (0.3Si, P)	M_2P ≫ MC
B10 (P, Si)	M_2P, Ni-rich γ	E10 (−Si, P)	M_2P ≫ MC
B11 (P, Ti, C)	M_2P ≫ MC ≫ $M_{23}C_6$	E11 (0.8Si, −Ti, 0.4Nb)	G ≫ NbC
B12 (P, Ti, C, Si)	M_2P ≫ MC > G > $M_{23}C_6$	E12 (0.3Si, −Ti, 0.4Nb)	NbC > G
B13 (Nb, C)	NbC	E13 (−Si, −Ti, 0.4 Nb)	NbC
B14 (0.01P)	No new phase	E14 (−Si, 0.1Ti, 0.2 Nb)	NbC, MC

[a] Nominal composition of base ternary B1 alloy is Fe–15Ni–13Cr and that of engineering E1 alloy is Fe–13Cr–15Ni–2Mo–2Mn–0.2Ti–0.04C–0.8Si. Added or omitted elements are indicated in the parentheses. Phosphorous additions are about 0.05 wt% unless specified. Small amounts of boron (< 0.002 wt%) were added in alloys B4 and B8.
[b] "−" signs next to the elements indicate that the alloying elements are subtracted from the master E1 alloy.

Table 2
Typical compositions of the precipitate phases formed during irradiation (at.%)[a]

Phases	Si	P	S	Ti	Cr	Mn	Fe	Ni	Mo	Nb	Reference alloys
$M_{23}C_6$	–	–	–	–	63	–	25	4	8	–	
	–	–	–	–	69	–	26	5	–	–	B12
η	12	–	–	–	33	–	19	28	8	–	E1
	11	–	–	–	33	–	19	14	23	–	E3
TiO	–	–	–	100	–	–	–	–	–	–	B2, B5
	–	–	–	93	2	–	–	–	5	–	B6
	–	–	–	84	6	–	10	–	–	–	B7
MC	–	–	–	55	39	–	6	–	–	–	B5
	–	–	–	27	21	–	15	–	37	–	B6
	[b]	–	–	59	26	–	15	–	–	–	B7
NbC	–	–	–	–	39	–	8	7	–	46	B13
	10	–	–	–	19	–	5	8	8	50	E12
M_2P	–	34	[b]	–	32	–	19	15	–	–	B9
	8	24	5	–	26	–	13	24	–	–	B10
	[b]	32	–	17	22	–	10	19	–	–	B11
	11	24	5	8	14	–	8	28	–	–	B12
	10	22	–	8	14	–	11	27	8	–	E8
	1	29	–	13	20	–	11	19	7	–	E10
G	22	2	1	4	11	–	6	54	–	–	B12
	38	–	–	4	7	6	6	34	5	–	E1
	24	–	–	4	7	7	6	47	5	–	E8
	28	–	–	–	6	7	6	44	4	5	E11
	20	–	–	–	6	7	6	50	3	8	E12
Ni-rich γ	4	–	–	–	9	–	44	43	–	–	B3
	10	–	–	–	8	–	40	42	–	–	B3
	4	–	–	–	9	–	52	35	–	–	B10
	9	–	–	–	13	–	51	27	–	–	B10
CrSi	42	–	–	–	43	–	14	1	–	–	B3

[a] Carbon and oxygen are not included in the carbide and oxide particle compositions.
[b] Trace or occasional inclusion.

FeTiP-type phosphides, which enhanced C in solution, such an increase did not occur during irradiation. Instead, profuse phosphide particles with modified compositions (high Cr but reduced Ti) developed during irradiation.

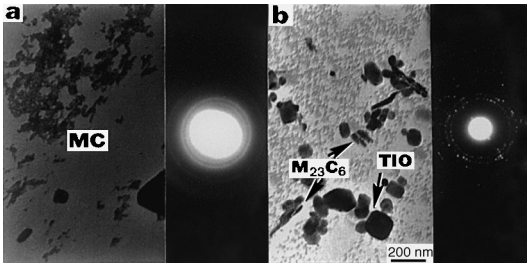

Fig. 1. (a) Extracted MC particles from the B6 alloy aged for six months at 948 K and the corresponding diffraction pattern, and (b) extracted TiO and $M_{23}C_6$ particles from the B6 alloy irradiated to 70 dpa at 948 K and the corresponding diffraction pattern.

3.2. Eta phase

The occurrence of η was suppressed by ion irradiation, and only a few particles were identified in alloys E1 and E3. During thermal aging, η phase readily developed in the alloy lacking titanium (E4) or in phosphorous containing alloys (E8, E9), but such enhancement was not found under ion irradiation. Profuse η precipitates were observed in a neutron irradiated (low damage rate) AISI 316 stainless steel [15,16] and in a pulsed ion beam irradiated Ti-modified austenitic stainless steel, similar to E1 alloy [17]. It may be that the suppression of η phase under ion irradiation is due to the high damage rate and shift of radiation induced segregation (RIS) relative to thermal diffusion effects rather than

insufficient thermal exposure during the irradiation period. In fact, the damage rate dependent stability of η phase was confirmed by the dissolution of the neutron irradiation induced η particles during subsequent Ni ion irradiation [18]. The composition of η phase was not altered by irradiation.

3.3. TiO

During irradiation, copious TiO particles developed in alloys B2 and E5, and to a much greater extent than during thermal aging. Although the former two alloys had no added carbon, surprisingly, TiO formation was enhanced even in alloys with carbon (B5, B6, B7, and B8). In the latter four alloys, small MC (or TiC) particles were also present but their volume fractions were noticeably reduced compared with thermally aged control specimens, indicating that there was a clear reversal of relative stabilities of the TiC to TiO phases under ion-irradiation. This phenomenon was not observed in the complex E-series alloys. When phosphorous was present, however, a Ti-rich phosphide was formed instead and TiO was suppressed.

Fig. 2 shows large cuboidal or rectangular TiO particles extracted from alloys B2 and E5 (no C addition), and B5 and B7 (0.04 wt% C). TiO particle sizes were smaller in alloys with carbon indicating that the growth of TiO particles was somewhat restrained by TiC formation. The electron diffraction patterns from these particles confirmed an fcc crystal structure with a lattice parameter $a = 0.42$ nm. The irradiation-produced TiO particles had somewhat more Cr, Fe, and Mo than thermally-produced TiO. As can be seen in Fig. 2(c), some TiO particles revealed an unusual cavity-like feature at the center of the particles. A similar hallow shape morphology was also observed in NbC particles in a thermally aged Fe–10Cr–6Mo–0.5Nb–0.05C ferritic steel [19]. The nature of these hallow regions has not been determined.

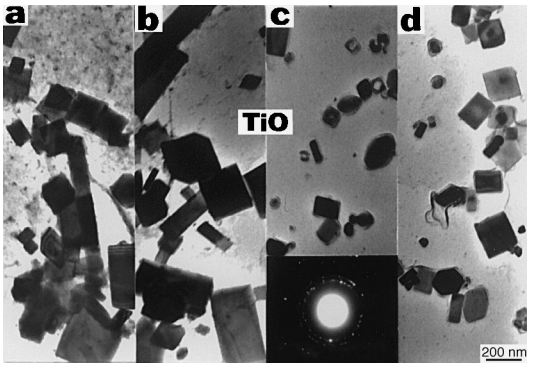

Fig. 2. TiO particles extracted from (a) B2, (b) E5, (c) B5, and (d) B7 alloys 4 MeV Ni-ion irradiated to 70 dpa at 948 K. The former two alloys have no carbon addition and the latter two have 0.04 wt% carbon. The insert is a diffraction ring pattern from the particles in alloy B5.

3.4. MC

Here, MC designates the TiC phase with various transition elements and does not include the Nb-rich carbide, NbC. A very high number density of fine MC particles (<10 nm) were nucleated rapidly during irradiation in all alloys that contained titanium and carbon. The rapid MC formation was due to profuse nucleation sites produced by radiation damage and to radiation-enhanced diffusion. Such a magnitude of MC formation did not occur in solution annealed alloys during thermal aging. The radiation-produced MC particles had a somewhat higher fraction of Cr, Fe, and Mo, but were otherwise virtually the same as the thermally formed MC. As mentioned above, when TiO formation (in B5, B6, B7, B8) became active under irradiation, MC was suppressed; this is an opposite trend to what was observed during thermal aging. In the presence of phosphorous, Ti-rich phosphide became dominant during irradiation and thus MC was reduced.

3.5. NbC

In alloys containing Nb and C, NbC particles precipitated copiously on the radiation-induced dislocations. NbC particles were somewhat coarser (<20 nm) than the MC formed in Ti-containing alloys. The nature of this NbC phase was different from thermally produced NbC in two aspects, namely precipitate size and composition. As the silicon concentration increased, the NbC particle size was refined and the volume fraction was also reduced. This was mainly because Si favored the formation of a Si- and Nb-rich G-phase, and thus niobium was depleted from solution. The radiation-produced NbC particles accommodated more foreign elements such as Cr, Si, and Ni compared to the NbC produced in the same alloy during thermal aging; Si and Ni were not observed in the thermally-produced NbC phase.

3.6. M_2P

In phosphorous-containing alloys, needle-shaped phosphide particles nucleated very rapidly on the loops and dislocations produced during irradiation, although phosphides were the slowest nucleating phase under thermal aging. At 1 dpa, phosphide precipitates were already dominant; such a scale of phosphide formation has not been observed under thermal aging conditions. MC was noticeably suppressed when the phosphide became dominant, partly due to the loss of Ti into the phosphide. Fig. 3 shows the phosphide microstructure at

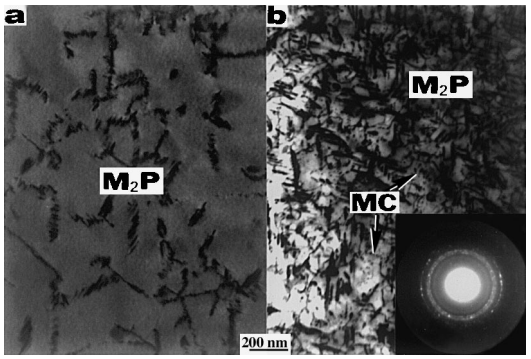

Fig. 3. M_2P precipitates in B12 alloy after (a) 1 and (b) 70 dpa irradiation at 948 K. The insert is a diffraction ring pattern obtained from the extracted particles.

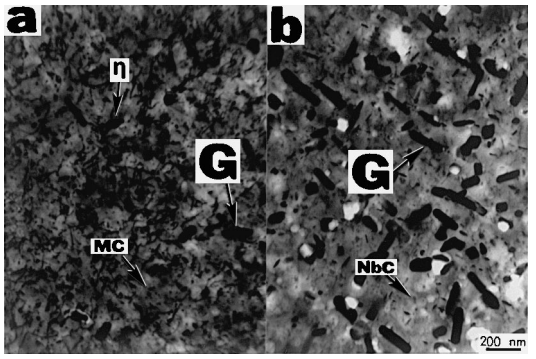

Fig. 4. G-phase particles in (a) E1 (Ti-modified) and (b) E11 (Nb-modified) alloys irradiated to 70 dpa at 948 K.

1 and 70 dpa. Phosphide particle sizes tended to coarsen in the absence of Ti (B9, B10), suggesting that an optimization of the Ti concentration is needed for the refinement of particle sizes and to achieve high precipitate number densities.

EDS analyses revealed that the phosphide compositions had higher Si and Ni concentrations than their thermal counterparts. Electron diffraction patterns from the extracted phosphide particles revealed an Fe_2P-type hexagonal structure, the same as for the thermal phase. Two typical phosphide compositions were found: a Cr-rich phosphide in alloys with no Ti addition (B9, B10) and a Ti-rich phosphide in titanium containing alloys (B11, B12, E8, E9, E10). Phosphide compositions showed an approximate $M_2(P,Si)$ stoichiometric relation where M represents metallic elements, Ti, Cr, Fe, Ni, and Mo. The assignment of Si to a P site was consistent with the report by Rundqvist [20] that Si substitutes on a P site. The phosphide phase accommodated a wide range of elements including S.

3.7. G-phase

G-phase developed in most of the E-series alloys with high Si, although it did not occur during thermal aging. G-phase compositions showed high Ni and Si with varying amounts of Ti, Cr, Mn, Fe, Mo, and Nb. The G-phase particles were generally nucleated near the center of the damage-induced interstitial loops, suggesting that segregation of Si and Ni at defect sinks led to the G-phase formation. EDS analysis confirmed an enrichment of nickel and silicon at such loops [21]. The G-phase was almost completely suppressed when the silicon level was reduced to below 0.3 wt%.

The G-phase was a unique phase which accommodated virtually all alloying elements, and yet not all of these elements were required for G-phase formation. A systematic elimination of alloying elements one at a time from the E1 alloy revealed that there was no particular single element essential for G-phase formation as long as there was enough Si and either Ti or Nb present. Of the latter two, niobium was the stronger G-phase promoter. As shown in Fig. 4, the distribution of G-phase is more extensive in E11 (0.4 wt% Nb, equivalent to 0.2 wt% of Ti in at.%) than in E1 (0.2 wt% Ti), although both alloys have the same base composition except for Ti and Nb. Niobium-rich G-phase was also found in a neutron-irradiated niobium-stabilized austenitic steel by Williams and Titchmarsh [16].

An atom probe field-ion microscopy study by Miller et al. [22] showed that (1 ± 0.7) atomic percent carbon was present in the G-phase particles in a CF 8 stainless steel. On the other hand, Williams and Titchmarsh [23] reported that carbon was unfavorable for G-phase formation because it promoted carbides. In this work, G-phase did not occur in alloy E5, which had all of the alloying elements except carbon, suggesting that the presence of carbon may be necessary for G-phase formation even though it is a silicide. It is, however, not clear whether carbon deficiency or other chemical effects prevented G-phase formation in E5 alloy, since Si and Ti concentrations were also reduced in this alloy due to the formation of γ' (Ni_3Si) and TiO.

3.8. Gamma prime

Gamma prime (γ') particles were observed only in alloy E5, which lacked carbon. Fig. 5 shows bright and dark field micrographs of γ' particles. The electron diffraction pattern showed that γ' particles had a cube on cube relation with the matrix and had an ordered $L1_2$ fcc structure. Unfortunately, the precise composition of γ' particles could not be determined because of difficulties in extraction. However, in-foil analysis of γ' particle compositions indicated an enrichment of Si and Ni. In other work [15], the compositions of γ' have been found to be approximately 65Ni–20Si–15(Cr,Fe,Mn). γ' was found to be a relatively pure Si- and Ni-rich phase

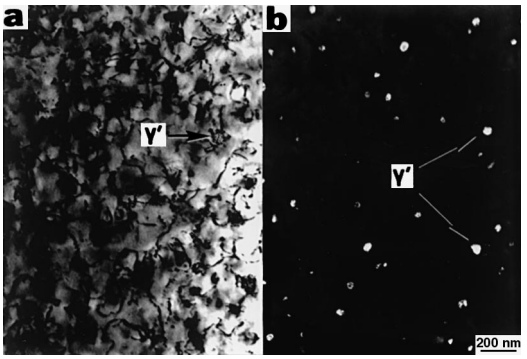

Fig. 5. γ' particles in E5 (no carbon addition) alloy irradiated to 70 dpa at 948 K.

compared with G-phase, which accommodates a greater fraction of transition elements such as Ti, Mo, and Cr. Of interest was that G-phase formation was inhibited at the expense of γ' in the E5 alloy, perhaps due to the absence of carbon in this alloy as mentioned already.

Although γ' phase has been frequently observed in AISI 316 type austenitic stainless steels neutron-irradiated at low temperatures (<550°C) [15,24,25], it has not been observed under heavy ion irradiation where a high damage rate and a high temperature (>500°C) are generally employed. In a separate irradiation for D9C1 alloy, similar to E1 but having higher silicon (1 wt%) and lower molybdenum (1.5 wt%), however, γ' formation was also observed under the same ion irradiation conditions used for B- and E-series alloys. Therefore, it is believed that γ' can form even under high damage rate ion irradiation and at higher temperatures, should the Si supersaturation be increased and G-phase formation be suppressed by lowering Mo.

3.9. Ni-rich-gamma

The composition of alloy B3 was chosen to examine the effect of silicon, namely by adding 0.8 wt% silicon to the base ternary. Surprisingly, the expected γ' phase did not develop in this alloy during Ni ion irradiation, but instead a high-nickel quaternary precipitate phase developed. EDS analysis revealed that a typical composition of the precipitates was 45Ni–42Fe–8Cr–5Si. The Si and Ni concentration in these precipitates were about six- and three-fold higher, respectively, compared with those in the matrix, 71Fe–15Ni–13Cr–0.8Si. The shape of the precipitates appeared generally as spheres or as a coating around cavities when He was coimplanted, often linking-up to form peanut-shaped dumbbells, suggesting that Si and Ni segregation around cavities or defects was the major cause for the formation of this phase. Cavity coatings have been observed also previously [25–28].

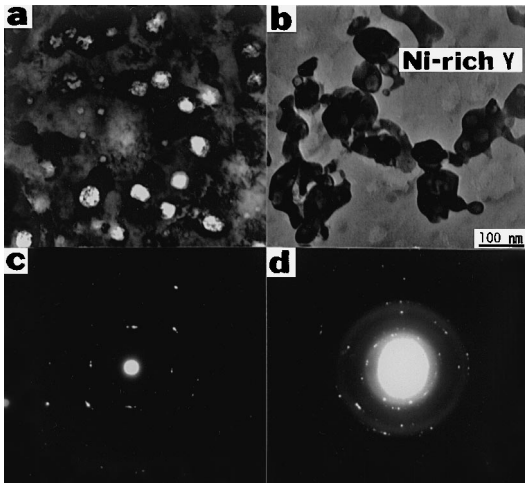

Fig. 6. Alloy B10 irradiated to 60 dpa with Ni-ions and 440 appm He at 948 K: (a) Ni-rich-γ coatings around the cavities, (b) extracted particles on carbon film.

The Ni-rich-γ phase developed also in alloy B10 although it had phosphorous in addition to silicon. The in-foil and extracted Ni-rich-γ particles are shown in Fig. 6(a) and (b), respectively, for alloy B10 irradiated to 60 dpa and 440 appm He at 948 K. Strain contrast around the precipitates is evident due to misfit. Fig. 6(c) and (d) show diffraction patterns for the in-foil and extracted particles, respectively. The diffraction patterns from the foils showed skewed spots superimposed upon the matrix diffraction pattern, indicating that the Ni-rich-γ phase had a skewed cube on cube orientation relative to the matrix due to coherent strain at the phase interface. The degree of misorientation increased as the particles grew. The electron diffraction rings from the extracted precipitates showed an fcc structure, the same as that of the matrix (γ), with the lattice parameter of $a = 0.356$ nm, i.e., about 1% smaller than that of the matrix.

3.10. CrSi

An unusual but quite abundant chromium silicide phase was also formed in alloy B3 (Si) during irradiation. This phase did not develop in alloy B10 (Si, P) because the phosphorous addition promoted phosphide formation. CrSi precipitates were not visible in the TEM foil and were identified from the extraction replica. EDS analysis revealed that the CrSi composition was typically 43Cr–42Si–14Fe–1Ni, having approximately equal Cr and Si stoichiometry. Besides the stoichiometric CrSi phase, there were small fractions of high-Cr phases with various Cr/Si ratios. The electron diffraction from these particles produced very complex powder ring patterns (Fig. 7) from which no specific crystallographic structure

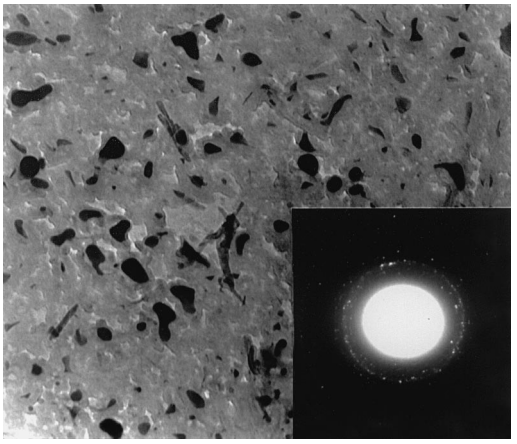

Fig. 7. Extraction replica of chromium silicide particles from B3 irradiated to 70 dpa at 948 K. The insert is a diffraction pattern from the extracted particles.

determination could be made at this time. The structure of CrSi is listed as cubic, FeSi B20 (space group T^4-P213) with lattice parameter $a = 0.462$ nm in Ref. [29].

4. Discussion

Phase transformations under irradiation are very complex phenomena and are affected by various intrinsic and extrinsic factors such as alloy composition, thermomechanical treatment, and irradiation conditions (temperature, damage rate, helium generation, etc.). In this work we have examined the phase stability in 28Fe–15Ni–13Cr alloys as a function of various alloying additions after irradiation with 4 MeV Ni ions at 948 K.

The results showed that there were four types of precipitate phases depending upon the solubility of silicon and nickel in the phases, similar to a pattern laid out in a previous publication [12]. Details are summarized below:

1. Si-free and low-Ni: thermal phases ($M_{23}C_6$, TiC, TiO);
2. high-Si and moderate-Ni: radiation modified phases (η, NbC, M_2P);
3. high-Si and low-Ni: radiation-induced phase (CrSi), and
4. high-Si and high-Ni: radiation-induced phase (G, γ', Ni-rich-γ).

The first type of precipitates are thermal phases whose compositions were not affected by radiation, but their formation was either enhanced or suppressed depending upon alloy composition. The second type of precipitates are radiation modified phases whose compositions were altered by radiation, but again their formation was either enhanced or suppressed depending upon alloy composition and irradiation conditions. The third and fourth types were truly radiation induced phases which were new phases that did not develop during thermal aging of these austenitic steels or similar stainless steels.

Interestingly, among the six thermally stable phases in the first two categories above, the non-carbide (M_2P, TiO) phases were enhanced by radiation, while the remaining four carbide phases ($M_{23}C_6$, η, MC, NbC) showed either enhancement or retardation depending upon the alloy composition. The formation of TiC and NbC was generally enhanced due to profuse nucleation sites produced by radiation damage combined with radiation-enhanced diffusion when there was sufficient carbon. In such a case, $M_{23}C_6$ and η were suppressed as a result of carbon depletion caused by MC formation. The stability of carbides was also affected by the formation of M_2P or TiO, because these phases compete for common solutes, C and Ti. For example, the formation of M_2P and/or TiO phase depleted titanium from solution leaving excess carbon in solution. This resulted in the suppression of MC and the promotion of $M_{23}C_6$.

Phosphide formation was extremely sluggish under thermal aging, but by contrast was remarkably enhanced by radiation. Diffusion coefficients of carbon and phosphorous in γ-iron at 1183 K (910°C) are 1.5×10^{-11} m^2/s and 3.6×10^{-16} m^2/s, respectively [30]. The sluggish formation of phosphide under thermal conditions is thus reasonable. The enhancement of the phosphides was, however, also observed in a high phosphorous (Fe–18Cr–10Ni–0.3P) austenitic stainless steel during quenching and aging experiments [31] This was a critical experiment which demonstrated that vacancy supersaturation and defects induced by quenching are primary reasons for the enhanced phosphide formation. Although the alloys investigated here had several times less phosphorous (0.05 wt%), it is believed that the enhanced diffusion by the increased vacancy supersaturation together with the defects produced by damage attributed to the rapid phosphide formation during irradiation. Furthermore, the high Si-affinity of phosphide encouraged its formation as Si segregated at defects under irradiation. In these ion-irradiation experiments, it was not determined whether the phosphide was a thermal equilibrium phase; i.e., whether the phosphide particles would dissolve again if annealed subsequently. However, an extensive development of phosphide was observed in MC-strengthened austenitic steels subjected to creep test at 700°C [32]. Similar results were observed in an AISI 321 stainless steel (0.03 wt% P) aged for 17 yr at 873 K [33], suggesting that phosphide is a thermal phase.

The NbC phase accommodated an unusually high silicon concentration and showed a refinement of its mean particle size with increasing silicon, but the volume fraction of NbC decreased as a Nb-rich G-phase

developed. This trend is consistent with the nature of competition for niobium between NbC and G-phase. Since the thermal NbC phase did not retain any silicon, it is believed that silicon segregation may have reduced NbC stability in favor of the Si-accommodating G-phase.

The η phase was suppressed during ion irradiation. This result is rather surprising because Si-segregation should have helped the formation of η phase since it has a high solubility for Si. As mentioned already, the damage rate is an important factor for the stability of η phase. It is a thermal carbide phase which requires high Cr, Mo, Si, and Ni. Therefore its stability appeared to be linked to the balance between radiation effects (Si, Ni segregation) and thermal effects (C, Cr, Mo segregation). An increase in damage rate without the corresponding increase in temperature may have reduced the ratio of (Cr, Mo)/(Si, Ni) at sinks, destabilizing the η phase. Moreover, η phase is a carbide and the enhancement of MC (depletion of C) under irradiation may have caused an adverse effect on the stability of η phase.

When thermal processes are sluggish, a true equilibrium state may be unobtainable in a given temperature range. In the vigorous damage environment, however, atoms are constantly displaced, replaced in lattice sites and reconstructed (i.e., each atom experienced on average 70 displacements after 70 dpa) and diffusion is enhanced by the increased point defect supersaturations, expediting the approach to an equilibrium state. Two such examples were observed in this experiment: (1) radiation-enhanced nucleation of phosphide as seen above, and (2) radiation catalyzed transition from a meta-stable TiC to a stable TiO phase.

During irradiation an unusual enhancement of TiO phase was observed. This process was accompanied by a reduction of TiC and a moderate increase in $M_{23}C_6$ phase in comparison to the thermal aging cases. The reversed stability from TiC (thermal) to TiO (radiation) raises the question of which phase is truly a thermally stable phase.

As briefly mentioned already, the source of oxygen for TiO is believed to come from oxide inclusions introduced during alloy melting; this was confirmed in Part I. In Fe–Cr–Ni austenitic steel, most dissolved oxygen exists in the form of chromium oxide because Cr_2O_3 is the most stable phase among Cr_2O_3, Fe_3O_4, and NiO [34]. Under thermal aging the formation of TiC proceeds rapidly because of the fast carbon diffusion, incorporating virtually all of the Ti into this tightly bound compound, while oxygen remains tightly bound in Cr_2O_3. The rates of back reactions releasing Ti and O are evidently negligible at the aging temperature of 948 K. However, under irradiation the atomic bonds are constantly broken in displacement cascades and the ejected atoms from all precipitates are free to diffuse through the matrix and to participate again in all possible reactions. The diffusion processes themselves are also radiation enhanced because of the high radiation-induced supersaturation of point defects. Calculations based on the Gibb's free energy of formation data reveal that TiO is a more stable phase than TiC under thermal conditions. However, it did not form during thermal aging because of low concentration of free oxygen in solution [35]. Under irradiation, however, the reaction between Ti and O is energetically favored because of the availability of oxygen released through cascade dissolution. While it is well known that irradiation can drive a system away from equilibrium, this result showed that irradiation also can catalyze the formation of a more stable phase at the expense of a persistent metastable phase.

There were four phases which were not found in aged specimens, but which are clearly induced by irradiation. These include G, γ′, Ni-rich-γ, CrSi, all rich in Si and/or Ni, showing that Si and Ni segregation during irradiation is a predominant factor in the formation of these particular phases. A verification of the radiation-induced nature of these phases can be made by post-irradiation annealing; G and γ′ phases have been found to dissolve back into solution during annealing at irradiation temperature [13–15]. Although post-irradiation annealing tests have not been carried out for Ni-rich-γ and CrSi phases, they are also believed to be radiation induced phases because they are not found in aged specimens, have unusually high silicon (i.e., 42 at.% in CrSi), and appear as coatings around cavities that are produced only during irradiation (Ni-rich-γ). It is well known that Si and Ni segregate at sinks by preferential solute-defect interactions during irradiation [7–10], thereby resulting in non-equilibrium phase formation. Of interest was that some Ni-rich-γ particles had >40% Ni, but had the same fcc structure and was still in the same γ phase region as the matrix. However, the abrupt phase boundary between matrix and coating indicates that there may exist a miscibility gap between the two distinct phase compositions.

Under neutron irradiation, Laves, η, and σ phases were enhanced and their formation temperature range extended downwards in AISI 316 and 316+Ti steels [12]. Thus these phases can be classified as radiation enhanced thermal phases. Such enhancement was, however, not observed with 4 MeV Ni or Fe ion irradiation. The suppression of these phase under ion irradiation are attributed to sluggish nucleation and growth rates. Extended defects formation and solute segregation under ion irradiation occur in a time scale less than a few hours while equivalent processes take place over several months to a few years for neutron case. Phases with slow kinetics seem to have not enough time to form under ion irradiation, before elemental resources and nucleation sites are exhausted by the formation of fast nucleating precipitate phases such as MC, M_2P, and G phase.

5. Conclusions

Precipitate phases in 28 different Fe–15Ni–13Cr austenitic stainless steels have been investigated as a function minor alloying additions after 4 MeV Ni^+ irradiation at 948 K. The results showed that irradiation caused either enhancement, retardation, modification, or creation of precipitate phases. Principal causes for these changes are attributable to the production of profuse precipitate nucleation sites (loops, dislocations, bubbles, cavities) introduced by radiation damage, the preferential segregation of Si and Ni at defects during irradiation, the radiation-enhanced diffusion by the increased point defect supersaturations during irradiation, and cascade induced mixing and dissolution of metastable phases. Although the phase stability during irradiation showed an extreme sensitivity to the changes in solute supersaturations as various precipitates evolved, Si and Ni segregation is a predominant factor for enhancing Si-accommodating phases and suppressing non-Si phases. Of particular interest was that, although MC formed readily in the complex E-series alloys during irradiation, TiO was favored over TiC in the simple B-series alloys. This is qualitatively different from either a radiation-induced departure from equilibrium or an enhancement of prevalent thermal phases. This is a novel situation in which the stable phase is not produced on thermal aging but only during irradiation, as a result of cascade mixing and dissolution and enhanced kinetics during irradiation.

Although the phase stability under irradiation is complicated, the results provide crucial insights into the energetics of the mechanisms involved, and provide a basis for tailoring alloy compositions to achieve controlled microstructures. For fission and fusion reactor structural materials applications, control of transmutation produced gas atoms is a very important issue in suppressing swelling. Fortunately, M_2P and MC particles can be developed in a fine scale with high number densities during irradiation if the alloy composition is tailored correctly. These are very desirable features because swelling can be suppressed via effective dispersion of gas atoms at the precipitate–matrix interfaces while mechanical strength can be improved by pinning dislocations by these particles [14,32,36–38]. To achieve this end, alloy compositions should be optimized by maximizing the dispersion of M_2P and MC particles.

Acknowledgements

This research was sponsored by the Division of Materials Sciences, US Department of Energy, under contract No. DE-AC05-96OR22464 with Lockheed Martin Energy Research Corporation. The authors wish to thank Dr P.J. Maziasz and Dr A.F. Rowcliffe for reviewing this manuscript.

References

[1] R. Sizmann, J. Nucl. Mater. 69&70 (1978) 386.
[2] R.S. Nelson, J.A. Hudson, D.J. Mazey, J. Nucl. Mater. 44 (1972) 318.
[3] P. Wilkes, J. Nucl. Mater. 83 (1979) 166.
[4] A.F. Rowcliffe, E.H. Lee, J. Nucl. Mater. 108&109 (1982) 306.
[5] P. Chu, N.H. Ghoniem, J. Nucl. Mater. 117 (1983) 55.
[6] A.A. Turkin, C. Abromeit, V. Naundorf, J. Nucl. Mater. 233–237 (1996) 979.
[7] L.E. Rehn, P.R. Okamoto, D.I. Potter, H. Wiedersich, in: Effects of Radiation on Structural Materials, ASTM 683 (1979) 184.
[8] V.K. Sethi, P.R. Okamoto, in: J.R. Holland, L.K. Mansur, D.I. Potter (Eds.), Phase Stability during Irradiation, AIME, 1981, p. 109.
[9] T.R. Allen, G.S. Was, E.A. Kenik, J. Nucl. Mater. 244 (1997) 278.
[10] S. Watanabe, N. Sakaguchi, K. Kurome, M. Nakamura, H. Takahashi, J. Nucl. Mater. 240 (1996) 979.
[11] P.J. Maziasz, C.J. McHargue, Int. Mater. Rev. 32 (1987) 190.
[12] E.H. Lee, P.J. Maziasz, R.F. Rowcliffe, in: J.R. Holland, L.K. Mansur, D.I. Potter (Eds.), Phase Stability during Irradiation, AIME, 1981, p. 191.
[13] P.J. Maziasz, J. Nucl. Mater. 205 (1993) 118.
[14] E.H. Lee, L.K. Mansur, Metall. Trans. 23A (1992) 1977.
[15] P.J. Maziasz, J. Nucl. Mater. 169 (1989) 95.
[16] T.M. Williams, J.M. Titchmarsh, D.R. Arkell, J. Nucl. Mater. 107 (1982) 222.
[17] E.H. Lee, N.H. Packan, L.K. Mansur, J. Nucl. Mater. 117 (1983) 123.
[18] A.F. Rowcliffe, E.H. Lee, P.S. Sklad, in: International Conference on Irradiation Behavior of Metallic Materials for Fast Reactor Core Components, Supplement, Ajacia, Corsica, 1979, p. 1.
[19] K. Farrell, E.H. Lee, Scripta Metall. 17 (1983) 791.
[20] Stig Rundqvist, Ark. Kemi 20 (7) (1962) 67.
[21] E.H. Lee, E.A. Kenik, J. Mater. Res. 3 (1988) 840.
[22] M.K. Miller, J. Bentley, in: G.J. Theus, J.R. Weeks (Eds.), Environmental Degradation of Materials in Nuclear Power System – Water Reactors, The Metallurgical Society, 1988, p. 341.
[23] T.M. Williams, J.M. Titchmarsh, J. Nucl. Mater. 98 (1981) 223.
[24] C. Cawthorne, C. Brown, J. Nucl. Mater. 66 (1977) 201.
[25] H.R. Brager, F.A. Garner, J. Nucl. Mater. 73 (1978) 9.
[26] P.R. Okamoto, H. Widersich, J. Nucl. Mater. 53 (1972) 336.
[27] D.J. Mazey, D.R. Harris, J.A. Hudson, J. Nucl. Mater. 89 (1980) 155.
[28] L.K. Mansur, W.G. Wolfer, J. Nucl. Mater. 69&70 (1978) 825.
[29] A. Taylor, B.J. Kagle, Crystallographic Data on Metals and Alloy Structures, Dover, New York, NY, 1963.

[30] R.W.K. Honeycombe, Steels Microstructure and Properties, American Society for Metals, Metals Park, Ohio, 1981, p. 7.
[31] A.F. Rowcliffe, R.B. Nicholson, Acta Metall. 20 (1972) 143.
[32] R.W. Swindeman, P.J. Maziasz, in: Proceedings of the Fifth International Conference on Creep of Materials, Lake Buena Vista, FL, USA, May 1992, p. 33.
[33] J. Bentley, J.M. Leitnaker, in: E.W. Collings, H.W. Kings (Eds.), The Metal Science of Stainless Steels, Met. Soc. AIME, 1978, p. 70.
[34] O. Kubaschewski, C.B. Alcock, Metallurgical Thermochemistry, 5th Ed., Pergamon, New York, 1979.
[35] E.H. Lee, L.K. Mansur, J. Mater. Res. 2 (1987) 291.
[36] L.K. Mansur, E.H. Lee, P.J. Maziasz, R.F. Rowcliffe, J. Nucl. Mater. 141–143 (1986) 633.
[37] W. Kesternich, J. Nucl. Mater. 127 (1983) 153.
[38] K. Herschbach, W. Schneider, K. Ehrlich, J. Nucl. Mater. 203 (1993) 233.